1 Propulsion & Control Systems Design

1.1 Propulsion Systems

1.1.1 Introduction

Building off of last year's rocket design iteration, the propulsion system consists of a solid rocket motor with a Rao contour nozzle. Constrained by last year's rocket dimensions, the combustion chamber can have a maximum diameter of 10". Motor casing and insulation is expected to fit within the proposed 2" increase in rocket diameter. The airframe design group has provided a rough estimate that this subsystem must be less than two meters long to be compatible with both rocket or plane models. Since last year's rocket accelerated up to speeds greater than Mach 8, the fuel grain geometry, nozzle geometry, and fuel composition must be re-evaluated to attain a desired flight profile.

1.1.2 Engine Configuration

There are two phases of flight that require thrust: the acceleration phase bringing the vehicle to a speed of Mach 3, and the cruise phase to maintain level flight and a constant speed during the supersonic test. A uniform fuel grain profile cannot meet the thrust requirements of both stages, therefore a two-phase profile is proposed. Illustrated in Fig. 1, the first phase consists of an annular grain geometry. This provides a large burn surface area and consequently a higher combustion pressure to generate more thrust. This is a progressive burn, meaning the combustion pressure increases due to the gradual increase in surface area as the inner surface burns outwards. Once the first phase has completely burned, there is a cylinder of fuel remaining in the combustion chamber. This is the second phase "end-burn" configuration which delivers a constant thrust to offset drag forces.

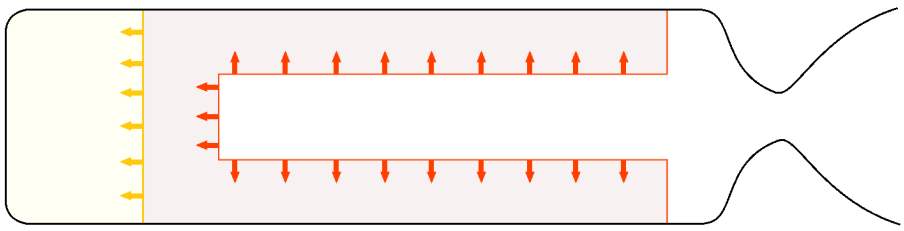

Figure 1: 2D illustration of the proposed two-phase fuel grain profile.

1.1.3 Thrust Model

The total thrust produced by a sounding rocket at a given altitude is defined by Eq. (1) below [1].

$$F_T = \dot{m}u_e + A_e\left(P_e - P_\infty\right) \tag{1}$$

The mission requirements specify that the rocket must operate a Mach 3 wind-tunnel at 70'000ft. This altitude is also the flight ceiling and hosts the test body for the longest time. For these reasons, initial engine sizing is based on the requirements of the cruise phase of flight. Furthermore, the acceleration grain has several flexible requirements and parameters such as its thrust, inner diameter, and time to Mach 3 while the cruise grain is far more rigid in terms of what is required and possible.

The exhaust mass flowrate and velocity are represented by Eq. (2) & (3) respectively [1]. These equations are valid for isentropic flow. The isentropic nozzle flow assumption is supported by last year's work which demonstrated a 2.6% difference between the thrust from an isentropic nozzle flow analysis versus a non-isentropic simulation [2]. Provided a fuel composition and its chemical properties, the density, ratio of specific heats (γ), gas constant (R), and flame temperature T_c are known. To simplify the analysis, the stagnation temperature (T_0) is assumed equal to T_c. This implies no energy is lost in the combustion process and complete combustion occurs.

$$\dot{m} = \frac{P_0 A_t \sqrt{\gamma}}{\sqrt{RT_0}}\left(\frac{2}{\gamma+1}\right)^{\frac{\gamma+1}{2(\gamma-1)}} \tag{2}$$

$$u_e^2 = \frac{2\gamma RT_0}{\gamma-1}\left[1-\left(\frac{P_e}{P_0}\right)^{\frac{\gamma-1}{\gamma}}\right] \tag{3}$$

Subsituting these equations into Eq. (1) yields Eq. (4) which has two unknown terms: P_0 and A_t. Nozzle exit area (A_e) is limited by the geometry of the vehicle. The nozzle exit diameter is set to 10" to maximize thrust while ensuring it does not extrude out into the freestream flow. The following section will expand on the stagnation pressure and further assumptions made.

$$F_T = \frac{2\gamma RT_0 P_0 A_t \sqrt{\gamma}}{(\gamma-1)\sqrt{RT_0}}\left(\frac{2}{\gamma+1}\right)^{\frac{\gamma+1}{2(\gamma-1)}}\left[1-\left(\frac{P_e}{P_0}\right)^{\frac{\gamma-1}{\gamma}}\right] + A_e\left(P_e - P_\infty\right) \tag{4}$$

1.1.4 Sizing Methodology

For preliminary solid rocket motor design, the velocity of combustion products at the exit of the chamber are often assumed neglible. This leads to the assumption that the static and stagnation pressures are equal [1][3]. Since stagnation pressure does not change without shocks, work, or heat transfer, this assumption's validity is reinforced by the fact that constant chamber pressure is needed

to achieve a constant thrust profile. This assumption is not valid for the increasing pressure expected over a progressive burn.

Solving for the combustion chamber pressure is possible using the conservation of mass and fuel properties.

$$\frac{dm_s}{dt} = \frac{dm_g}{dt} + \dot{m}_e \tag{5}$$

Eq. (5) is a conservation of mass model of the combustion chamber. The change in solid fuel mass $\frac{dm_s}{dt}$ as it burns is equal to the sum of the change in gas mass within the combustion chamber $\frac{dm_s}{dt}$ and the nozzle mass flowrate out of the chamber $\dot{m}_e$. The flowrate out of the nozzle has already been represented by Eq. (2). The solid mass change can be modeled by a simple massflow equation (6) which relies on fuel density, geometry, and surface burn rate $\dot{r}_{fuel}$.

$$\frac{dm_s}{dt} = \rho_s \dot{r}_{fuel} A_b \tag{6}$$

$$\frac{dm_g}{dt} = V_g \frac{d\rho_g}{dt} + \rho_g \frac{dV_g}{dt} \tag{7}$$

A gas' mass change in the combustion chamber can be expressed by Eq. (7), where V_g is the instantaneous gas volume and ρ_g is the instantaneous gas density [1]. From the thrust equation, it is evident that to maintain constant thrust at a fixed altitude, fuel, and nozzle geometry, the combustion chamber pressure must remain constant. This ideal scenario is enforced in the analysis of the cruise burn, although in practice it is not possible without a variable nozzle geometry. Referring back to earlier assumptions, isentropic flow follows the ideal gas law $P = \rho RT$. The density of the gas will not change if the pressure remains constant, hence the density rate of change term in Eq. (7) is eliminated. The volume rate of change term is negligible due to the relatively low density of the gaseous combustion products ($\rho_g << \rho_s$)[4]. As a result, the change in gas mass within the combustion chamber can be totally neglected during the simplified analysis of the cruise burn. Expanding Eq. (5)'s remaining terms and re-arranging for combustion pressure results in the following formula:

$$P_c = P_0 = \frac{\rho_s \dot{r}_{fuel} A_b}{A_t} \sqrt{\frac{RT_0}{\gamma} \left(\frac{\gamma+1}{2}\right)^{\frac{\gamma+1}{\gamma-1}}} \tag{8}$$

$$P_c = P_0 = \rho_s \dot{r}_{fuel} C^* \frac{A_b}{A_t} \tag{9}$$

The square root portion of this expression is solely dependent on fuel properties and is refered to as the characteristic velocity C^*. Eq. (8) is reduced to Eq. (9) which is identical to the combustion pressure formula specified by NATO for preliminary solid rocket motor design [3]. While it could've been directly used from [3], it is important to understand the assumptions that were

used to formulate this expression.

The constant gas volume and density simplifications cannot be applied to the acceleration burn which is expected to have an increasing chamber pressure as it burns radially outwards. Expanding and re-arranging Eq. (5) without neglecting the gas mass rate of change yields the following differential equation:

$$\frac{v_g}{RT^o}\frac{dP}{dt} + \rho_g \dot{r}_b A_b = \rho_s \dot{r}_b A_b - \frac{PA_t}{C^*} \tag{10}$$

Both this equation and Eq. (9) involve a time-varying fuel burn rate $\dot{r}_b$. The burn rate of a fuel is proportional to the combustion pressure. A common approach to modeling the relationship between burn rate and pressure is Eq. (11) where n is a unitless parameter known as the pressure exponent and a is the temperature coefficient with units $\frac{m/s}{Pa^n}$ [1][4]. Both parameters are empirically determined. The pressure exponent value tends to lie between 0 and 1. The pressure sensitivity of the burn rate increases as the pressure exponent approaches unity. Subsituting Eq. (11) into Eq. (9) and re-arranging the formula yields the final equation (12) for a constant combustion chamber pressure. Likewise, substituting Eq. (11) into Eq. (10) and re-arranging the formula yields the final differential equation (13) modeling combustion chamber pressure.

$$\dot{r}_b = aP^n \tag{11}$$

$$P_c = P_0 = \left(a\rho_s C^* \frac{A_b}{A_t}\right)^{\frac{1}{1-n}} \tag{12}$$

$$\frac{dP}{dt} = \frac{aA_b\left(\rho_s - \rho_g\right)RT^o}{V_g}P^n + \frac{RT^oA_t}{V_gC^*}P \tag{13}$$

For any given burn area and set of fuel properties, the thrust equation (4) is used to solve for A_t to attain the required cruise thrust. The length of the cruise burn can be modified to increase or decrease the duration. The acceleration burn's grain geometry must then be tuned to meet the following conditions:

- The vehicle reaches a speed of Mach 3 at the end of the acceleration burn
- The combustion chamber pressure does not exceed 15MPa at any point during operation [4]

While the outer diameter remains the same as that of the cruise burn grain geoemtry, the length and the inner radius of the acceleration burn geometry can be tuned to produce sufficient thrust to meet the conditions above.

1.1.5 Simulation & Solver Approach

This section outlines the computational methodologies developed to simulate, optimize, and analyze fuel grain geometry. The approach integrates the analytical models from Sections 1.1.3 and 1.1.4 into a numerical framework, addressing

challenges such as time-varying combustion pressures, burn area evolution, and feasibility of various fuels. By leveraging MATLAB-based numerical solvers and optimization algorithms, the simulation system resolves coupled ordinary differential equations (ODEs) governing combustion pressure and burn rate, while also adhering to constraints like a maximum chamber pressure to ensure the motor design achieves Mach 3 flight without exceeding structural or operational boundaries. Fig. 2 presents an overview of the solver's operational flow. All of the MATLAB code can be obtained at https://github.com/ahm23/rocket-flight-sim-analytical.

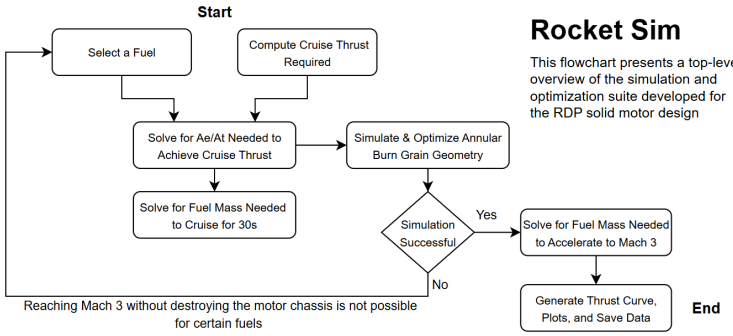

Figure 2: Overview of the solution process for the fuel grain geometry, nozzle geometry, and rocket motor thrust curve.

1.1.5.1 Cruise Burn Solver & Optimization Strategy

As previously noted, in this analysis the thrust equation (4) has two unknowns, P_0 and A_t. P_0 is computed using Eq. (12). P_e is dependent on the nozzle exit Mach number (M_e) as expressed by Eq. (14). Furthermore, M_e can be related to the expansion ratio (ε) as shown in Eq. (15) [1].

$$P_e = P_0 \left(1 + \frac{\gamma - 1}{2} M_e^2\right)^{-\frac{\gamma}{\gamma - 1}} \tag{14}$$

$$\frac{A_e}{A_t} = \varepsilon = \frac{1}{M_e} \left[\left(\frac{2}{\gamma + 1}\right)\left(1 + \frac{\gamma - 1}{2} M_e^2\right)\right]^{\frac{\gamma+1}{2(\gamma-1)}} \tag{15}$$

There is no straightforward closed-form expression for M_e in Eq. (15), therefore M_e and consequently P_e are computed over a discrete set of expansion ratios instead of using a direct solution for P_e with respect to A_t. Furthermore, A_t in the thrust equation (4) is replaced by A_e/ε. A discrete set of cruise thrust values can now be determined over the set of expansion ratios used for P_e. Finally, the expansion ratio needed to meet cruise requirements can be interpolated from this data at the point where the thrust is sufficient to offset drag. With that, the nozzle geometry is resolved and fixed for the acceleration burn analysis.

1.1.5.2 Acceleration Burn Solver & Optimization Strategy

Solving the differential equation (13) for combustion pressure over time is not as simple as feeding it into a MATLAB ODE solver like ode23 or ode45. The burn area for an annular grain geometry at any point in time can be expressed by Eq. (16). To solve for the burn area at any given time, the time-varying burn rate must be integrated from $t = 0$ up to the solution time to determine the total deformation of the inner radius (r_{in}). The cylindrical volume term V_g is also dependent on the total deformation of the inner radius.

$$A_b(t) = 2\pi r_{in} L = 2\pi \left(r_0 + \int_0^t \dot{r}_b dt \right) L \tag{16}$$

The approach used in this analysis defines both A_b and V_g as functions of r_{in}. The rate of deformation of r_{in} is the burn rate which can be directly related to chamber pressure as previously expressed by Eq. (11). With this rate of inner radius change over time, a system of ODEs can be formed and resolved by MATLAB.

$$\begin{cases} \frac{dr_{in}}{dt} = aP^n \\ \frac{dP}{dt} = \left[aA_b\{r_{in}(t)\}\rho_s \left(\frac{RT^o}{V_g\{r_{in}(t)\}} \right) \right] P^n + \left[\frac{A_t\sqrt{\gamma RT^o}}{V_g\{r_{in}(t)\}} \left(\frac{2}{\gamma+1} \right)^{\frac{\gamma+1}{2(\gamma-1)}} \right] P \end{cases} \tag{17}$$

The inner cross-section (base of the tube) and the outer cross-section (end of the tube) are assumed to burn at the same rate; hence, the length of the acceleration grain geometry remains constant throughout the burn and does not need an expression included in Eq. (17). The initial conditions of this system are the initial pressure (ambient pressure) and the initial inner radius.

An optimization script was developed to determine at what length the acceleration burn can produce favorable conditions to reach Mach 3 flight. Fig. 3 presents a flow chart of the script's operation.

Details on the computer programming methodologies, such as implementing an efficient algorithm for iterative optimization rather than just an incrementing loop, are beyond the scope of this report. Details on the flight simulation used to determine if the rocket achieves Mach 3 can be found in Section 1.2 of this report. Several HTPB-based fuels were trialed due to their composition flexibility and high energy density [4]. A limit of 15MPa is imposed on the chamber presssure since solid rocket motors on the high-end of the combustion pressure spectrum tend to generate around 12-14MPa [4].

1.1.6 Simulation Results

After evaluating six candidate fuels, the optimization software identified two fuels that could fullfil the mission requirements under certain configurations. The two compatible fuels are HTPB/AP[75%] + Fe2O3[3%] and HTPB/AP[70%]. These two fuels will be refered to as the "validated fuels". Table 1 summarizes

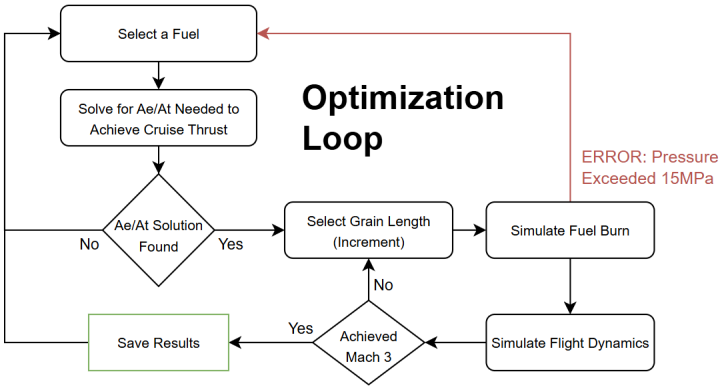

Figure 3: Overview of the optimization script's motor tuning and fuel selection.

the corresponding motor dimensions, mass, nozzle expansion ratio, and the time required to reach Mach 3 for each validated fuel. Included in the total motor length is the fuel grain length in addition to motor components. The motor hardware and igniter volume is expected to be no more than 15cm long.

Table 1: Motor Specifications Using Optimizer-Validated Fuels

Parameter	**HTPB/AP[75%]+Fe2O3[3%]**	**HTPB/AP[70%]**
Total Motor Length	1.41m	1.38m
Motor Diameter	0.254m	0.254m
Motor Mass Mass	118.6kg	116.1kg
Nozzle Expansion Ratio	10.06	22.08
Time to Mach 3	4.6s	11.5s

1.1.6.1 Inputs

Rocket parameter inputs based on the previous year's design iteration are summarized in Table 2. As the optimizer refines the rocket design, the body length is expected to decrease. This reduction in length will lower the wetted surface area, thereby reducing both lift and drag.

Table 2: Initial & Estimated Rocket Body Specifications

Parameter	**Value**
Length	3m
Diameter	0.254m
Mean Drag Coefficient	0.905
Dry Mass	253.8kg
Estimated Lift Required	2'559N

The fuels trialed and their burn rate parameters properties are tabulated in Table 3. The parameters of the first 5 fuels are sourced from a journal publication on defence technology [5]. Most are mixtures of HTPB and certain percentage of ammonium perchlorate as an oxidizer. Some of the fuels have ferric oxide in their composition which is known to increase the fuel burn rate [4]. The average density, specific heat ratio, gas constant, and flame temperature of HTPB fuels are 1854.55kg/m^3, 1.25, 320J/kgK, and 3440K respectively. HTPB2021 is the fuel used on this project two years ago for testing and its density is known to be 1740kg/m^3.

Table 3: Fuel Burn Rate Coefficients [5][2]

Fuel	**Temp. Coefficient** $\frac{m/s}{Pa^n}$	**Pressure Exponent**
HTPB/AP(80%) + Fe_2O_3(3%)	1.4595e-5	0.52
HTPB/AP(80%)	2.5714e-5	0.433
HTPB/AP(75%) + Fe_2O_3(3%)	1.1892e-4	0.323
HTPB/AP(75%)	7.6684e-4	0.136
HTPB/AP(70%)	0.0016	0.098
HTPB 2021	7.2500e-5	0.29

1.1.6.2 Cruise Grain Analysis Results

The thrust required to maintain Mach 3 flight at 70,000ft is approximately 1.28kN, with a standard deviation of 60N. This small variation is primarily due to the different fuel masses required for each type of fuel. The optimizer employed the cruise analysis methodology to determine the necessary nozzle expansion ratio for achieving the required thrust, based on interpolation of data presented in Fig. 4. The final cruise grain's geometric parameters and mass are summarized in Table 4.

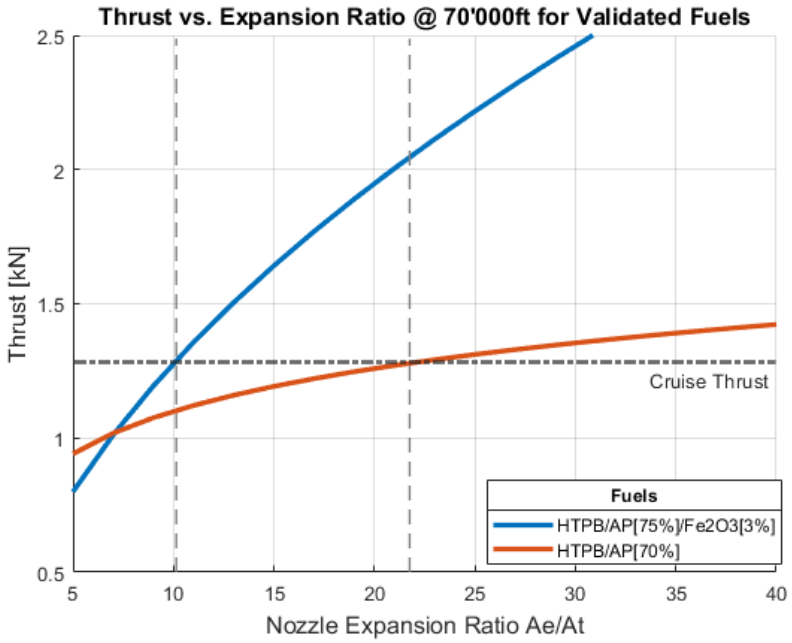

Figure 4: Thrust produced over a range of expansion ratios for two validated fuels in an end-burn configuration.

Table 4: Geometry and Mass of the Cruise Fuel Grain

Parameter	**HTPB/AP[75%]+Fe2O3[3%]**	**HTPB/AP[70%]**
Length	0.16m	0.15m
Diameter	0.254m	0.254m
Mass	14.91kg	14.07kg

Fig. 5 & 6 present thrust data over a range of expansion ratios for various smaller end-burn diameters. The HTPB/AP(75%) + Fe2O3(3%) formulation appears suitable to maintain cruise conditions with a smaller diameter and greater expansion ratio, resulting in reduced volume and mass; however, once tested with a higher expansion ratio, the acceleration burn failed to achieve Mach 3 flight without exceeding a 15 MPa chamber pressure.

The validity of the assumptions made in the cruise burn analysis methodology, such as negligible volume change and constant pressure, was proven by applying the acceleration burn analysis' methodology. Instead of an inner radius increasing over time at the burn rate, the length of the cruise burn decreasing at the burn rate is used as the second differential equation. The simplified and

more computationally efficient cruise analysis methodology yielded on average a 0.6% lower cruise thrust.

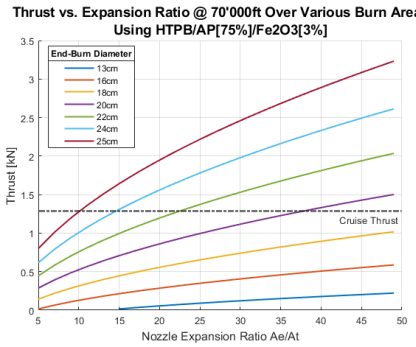

Figure 5: Thrust vs. expansion ratio for various end-burn configurations using HTPB/AP(75%) + Fe2O3(3%).

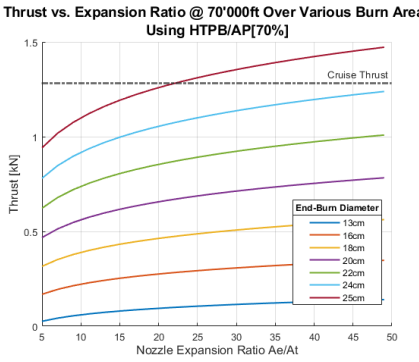

Figure 6: Thrust vs. expansion ratio for various end-burn configurations using HTPB/AP(70%).

1.1.6.3 Two-phase Grain Analysis Results

Acceleration grain parameters, mass, and maximum chamber pressure outputs from the optimizer are tabluated for both validated fuels in Table 5.

Table 5: Geometry and Maximum Pressure of the Acceleration Grain Phase

Parameter	**HTPB/AP[75%]+Fe2O3[3%]**	**HTPB/AP[70%]**
Length	1.26 m	1.23 m
Initial Inner Radius	4.35cm	4.35cm
Outer Radius	12.7cm	12.7cm
Mass	118.61 kg	116.12 kg
Max. P_c	14.28 MPa	9.78 MPa

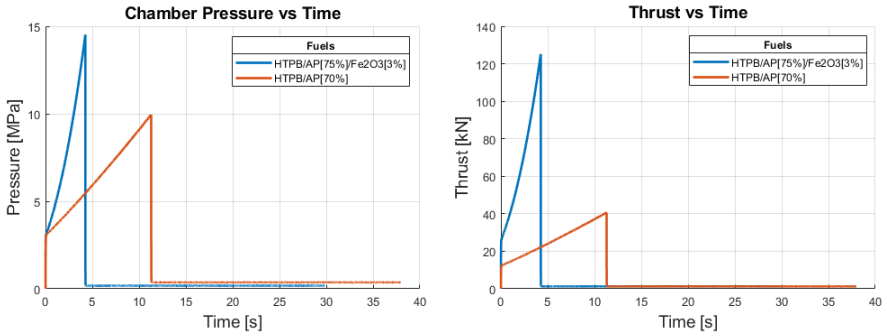

Figure 7: Motor chamber pressure and thrust curves for both validated fuels.

The chamber pressure and thrust curves are presented in Fig. 7. The change in fuel mass throughout the burn can be observed in Fig. 8. In all of these plots it is evident where the rocket motor transitions from acceleration to cruise operation with abrupt changes in rate of change and/or magnitude.

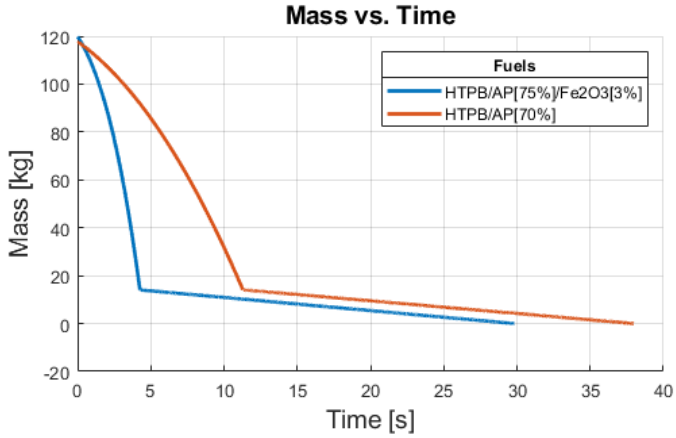

Figure 8: Remaining fuel mass over the burn duration for both validated fuels.

1.1.7 Conclusions

The propulsion system design successfully addressed the mission requirements by developing a two-phase solid rocket motor optimized for Mach 3 flight at 70'000ft. The annular grain geometry in the acceleration phase provided the necessary thrust to achieve Mach 3, while the end-burn configuration in the cruise phase ensured stable thrust to maintain level flight. The solver system demonstrated robustness in optimizing motor dimensions and nozzle geometry while adhering to requirements and constraints. Through rigorous analysis and numerical simulations, two fuel formulations HTPB/AP[75%] + Fe2O3[3%] and HTPB/AP[70%] were validated, with the latter offering a more conserva-

tive chamber pressure profile. Despite being capable of meeting the mission requirements, HTPB/AP[75%] + Fe2O3[3%] yields thrust forces that are too great for the airframe of the rocket.

Future improvements could explore slightly weaker fuel compositions to fine-tune performance. The initial inner radius of the acceleration fuel grain could also be tuned; however, the optimization script would need more sophisticated algorithms such as an implementation of quasi-newton numerial optimization methods [6]. Lastly, various other acceleration and cruise grain geometries could be analyzed with a simulator that follows a more computational geometry-focused approach rather than having to define a geometry using equations.

1.2 Trajectory Analysis

1.2.1 Introduction

A new simulation has been developped with the intention of providing more accurate results and resolving the shortcomings of the legacy simulation from last year's work. Those shortcomings include coupling of the rocket pitch with the flight's direction and a faulty integration of control surfaces. The anticipated launch height remains at 70'000ft (21.34km) as well as the rocket's dry mass of 253.80kg.

1.2.2 Simulation Appraoch

The net forces on the rocket body are computed at each time-step using Eq. (18) and (19). These forces are translated into accelerations using the total mass of the rocket and newton's second law of motion. Acceleration is integrated for velocity which is integrated for the position of the rocket throughout its trajectory. At the time of the development of this simulation, control systems were not completely defined; hence the rocket's pitch during acceleration follows a cubic-weighted smoothstep sequence between the launch angle and desired angle of attack at Mach 3, mimicking a PID controller. The fuel mass from ignition to burnout is computed by the rocket motor burn simulation and fed into the trajectory simulation to solve for the rocket weight over time.

$$\sum F_x = F_T sin(\phi) - F_D sin(\phi) - F_L cos(\pi + \phi) \tag{18}$$

$$\sum F_y = F_T cos(\phi) - F_D cos(\phi) - F_L sin(\phi) \tag{19}$$

A simple drag formula (20) is used to compute the drag force using an average of last year's simulated drag coefficient and the rocket cross-section area. At the time of writing, the average drag coefficient for this rocket is 0.9. This coefficient is expected to change with the new test section design. Likewise, a simple lift formula (21) is used to compute the lift force using last year's rocket geometry to determine the lifting area beneath the rocket. The lift coefficient required

is estimated in the following section on thrust profile evaluation. Atmospheric conditions are sourced from the International Standard Atmosphere model.

$$F_D = \frac{1}{2} C_D u^2 A_{ref} \tag{20}$$

$$F_L = \frac{1}{2} C_L u^2 A_{ref} \tag{21}$$

1.2.3 Simulation Results

Assuming the thrust vector is level with the horizon during cruise, the engine needs to generate enough thrust to offset any drag forces that would deccelerate the vehicle. Lift forces from fins and wings at Mach 3 are expected to offset the 2559N weight of the body. Computations using Eq. (21) indicate that a lift coefficient of at least 0.0734 is required. During cruise, a drag force of 1282N is estimated by the drag equation (20).

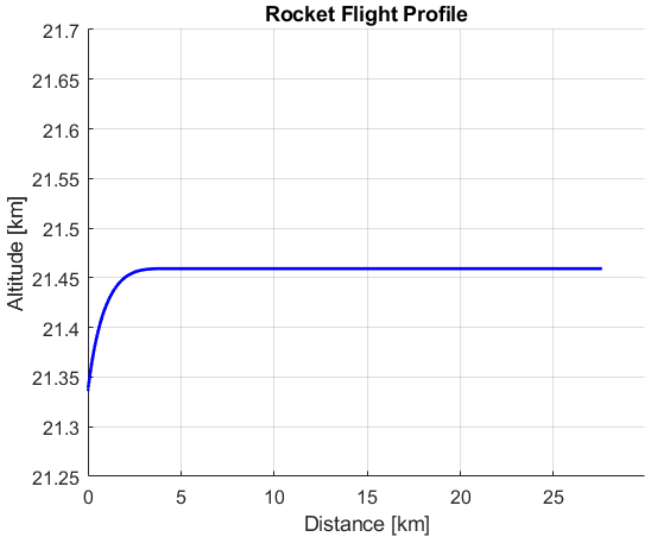

Figure 9: Rocket flight profile (excluding descent).

Using the motor configuration and thrust curve for HTPB/AP70% fuel (see Section 1.1.6), as well as a launch angle of 28° from the horizon, the rocket follows the flight profile plotted in Fig. 9. The rocket travels a distance of 27.6km prior to burnout. The descent phase of flight has yet to be analyzed.

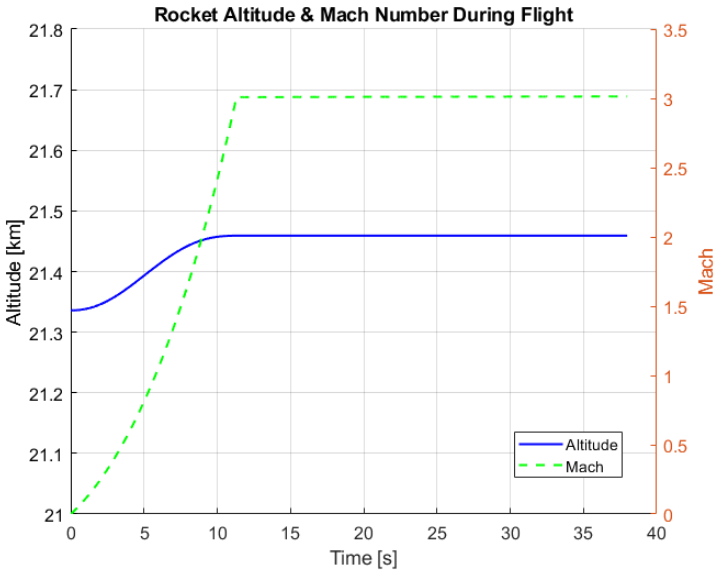

Figure 10: Rocket altitude and pitch profiles over flight time.

Fig. 10 presents the altitude and Mach number of the rocket over time. The altitude deviates 123m upwards from the 70'000ft launch position due to the initial launch angle and loss of fuel mass. As the rocket loses mass during cruise, exccess lift is generated since the rocket is expected to generate enough lift to carry its full initial weight. The time to Mach 3 is 11.5s and cruise Mach number deviated by a neglible 0.014 during cruise.

Net force and the various force components are plotted in Fig. 11. As expected, the lift and drag forces remain nearly constant throughout the cruise flight. The initial thrust component in the vertical direction (Y-axis) is due to the inclined launch angle which was necessary to use some thrust to prevent the rocket from free-falling uncontrollably.

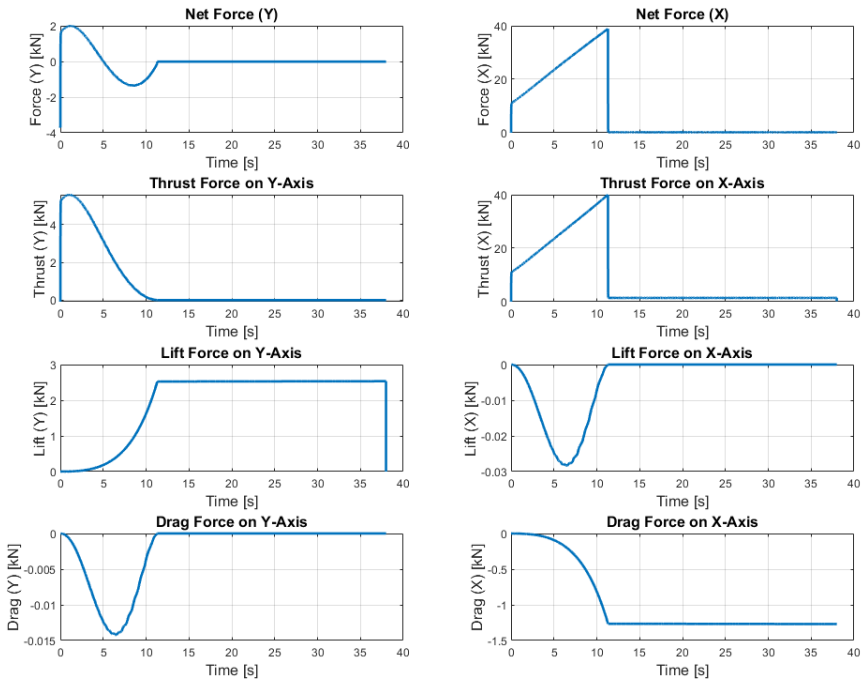

Figure 11: Net force, thrust, lift, and drag components acting on the rocket over the duration of flight.

1.2.4 Conclusions

The trajectory simulation provided a reliable assessment of the rocket's flight profile, confirming its ability to reach and sustain Mach 3 cruise conditions at 70,000 ft. Key findings include a minimal altitude deviation of 123 m during cruise, attributed to decreasing fuel mass and excess lift generation. The thrust and drag forces balanced effectively, ensuring near-constant velocity, while the launch angle of 28° facilitated stable ascent.

For future iterations of the simulator, it is important to take into account individual drag components. Wave drag and skin drag tend to vary significantly with Mach number. Furthermore, if a plane body is selected by the airframe design group, the total drag is likely to increase significantly due to the increased surface area of the wings. The next iteration will also include forces from vehicle control surfaces once they are defined. Overall, the results validate the feasibility of the mission, though additional analysis of the descent phase and refined force models will be critical for the next stages of development.

References

[1] J. Etele, *Fundamentals of Transatmospheric & Space Propulsion*. Aldanox Group Inc., 2022.

[2] J. Dubeau *et al.*, "Rocket propelled windtunnel," Carleton University, Tech. Rep., 2024.

[3] P. Kuentzmann, "Introduction to solid rocket propulsion," Office National d'Etudes et de Recherches Aérospatiales, Tech. Rep., 2004. [Online]. Available: https://apps.dtic.mil/sti/pdfs/ADA425146.pdf.

[4] G. P. Sutton and O. Biblarz, *Rocket Propulsion Elements*. Wiley, 2017.

[5] A. Manash and P. Kumar, "Comparison of burn rate and thermal decomposition of ap as oxidizer and pvc and htpb as fuel binder based composite solid propellants," *Defence Technology*, vol. 15, no. 2, pp. 227–232, 2019, ISSN: 2214-9147. DOI: https://doi.org/10.1016/j.dt.2018.08.010. [Online]. Available: https://www.sciencedirect.com/science/article/pii/S2214914718301946.

[6] J. Su, *Quasi-newton methods*, 2020. [Online]. Available: https://optimization.cbe.cornell.edu/index.php?title=Quasi-Newton_methods.